COMPARISON OF WIND SPEED MEASUREMENTS OVER THE OCEANS WITH THE SPECIAL SENSOR MICROWAVE/IMAGER AND THE GEOSAT ALTIMETER.

Nelly M. Mognard[1] and Kristina B. Katsaros[2]

[1] Centre National d'Etudes Spatiales
Groupe de Recherche de Géodésie Spatiale
Toulouse, France

[2] Dept. of Atmospheric Sciences
University of Washington
Seattle, WA USA

1. INTRODUCTION

The Geosat radar altimeter, and the Special Sensor Microwave /Imager (SSM/I) have been used successfully to identify, locate, and analyze the evolution of atmospheric fronts and polar lows (Mognard and Katsaros, 1990; Claud et al., 1991). Using a combination of sequential passive and active microwave satellite sensors yields new insights on the location and the evolution of these atmospheric systems that cannot be obtained by more conventional (in-situ or visible and infra-red) instruments. These satellite microwave sensors will in the near future be used to provide input data for atmospheric and sea state numerical models. The Seasat satellite, that worked from June to October 1978, was the first satellite to have flown an ensemble of passive and active microwave instruments among which three: the altimeter, the scatterometer, and the Scanning Microwave Multichannel Radiometer (SSMR) gave estimates of the ocean wind speed. Comparison of the three wind speed estimates from Seasat showed that significant biases were present in the retrieved wind speed (Mognard and Campbell, 1984).

In order to compare wind speed estimates from the Geosat altimeter and the SSM/I, 25 colocated passes, within 2 hours of each other, have been selected and the SSM/I estimates of wind speed and atmospheric parameters extracted along the Geosat track. Both instruments and their algorithms are described in section 2. In section 3, a statistical comparison of wind speed estimates is presented and the effects of the atmospheric parameters derived from SSM/I, and of the sea state parameters from Geosat are analyzed. Quasi-simultaneous measurements by Geosat and SSM/I, along a Geosat track in the North-East Pacific, are presented in section 4.

2. THE INSTRUMENTS AND THEIR ALGORITHMS

2.1 The Special Sensor Microwave/Imager

SSM/I consists of seven separate radiometers which simultaneously measure the upwelling polarized microwave emission from the Earth and its atmosphere at four frequencies: 19.35, 22.2, 37, and 85.5 GHz. The spatial resolution ranges from 55 km at 19 GHz to 15 km at 85 GHz. A detailed description of the instrument is given by Hollinger et al. (1987).

The algorithms used in this paper for estimating atmospheric water vapor, liquid water, index of precipitation, and ice scattering index are by Petty and Katsaros (1990a). Estimates of integrated water vapor content (IWV) are obtained from a regression of brightness temperatures at 19 and 22 GHz. Integrated cloud liquid water content (ICLW) estimates use a combination of the 37 GHz vertically and horizontally polarized channels. The determination of the index of precipitation (P37) is based on the 37 GHz normalized polarization method of Petty and Katsaros (1990b) developed with the SMMR on Nimbus-7. As was the case with SMMR, P37 < 0.8 occurs only in the presence of precipitation, while P37 > 0.9 generally implies precipitation-free pixels. The P37 index of precipitation is used to identify all regions of rain, including stratiform and warm-cloud rain at 25 km resolution. An estimate of the concentration and size of frozen precipitation particles above the freezing level P85 is derived from a linear combination of brightness temperatures at 85 GHz and provides high resolution(15 km) estimates of the location and relative intensity of cold-cloud precipitation (Petty, 1990).

The Global D-Matrix algorithm of Goodberlet et al., 1989 (which uses a linear combination of the 19, 22, and 37 GHz channels) is used to retrieve the ocean surface wind speed in regions with no precipitation. Comparing SSM/I wind speed estimates to measurements from buoys in the National Data Buoy Center (NDBC) network, Goodberlet et al. (1989), obtained no bias and standard deviations ranging between 1.4 to 1.9 m/s with collocation within 25 km and 30 minutes.

The SSM/I wind speed estimates are compared to the Geosat radar altimeter measurements along the altimeter track. The atmospheric parameters deduced from the SSM/I are used to classify the data.

2.2 The Geosat radar altimeter

The Geosat altimeter is a short-pulse (3.125 ns) nadir-viewing radar operating at 13.5 GHz. The Geosat radar altimeter system is described by McArthur et al. (1987). The sea state estimates deduced from the radar altimeter and used in these analyses are the ocean backscatter coefficient derived from the automatic gain control loop used to normalize the amplitude of the ocean return signal, and the significant wave height

(SWH) computed on board the satellite from the slope of the mean return waveform edge. The Geosat sea state estimates are available every second or every 6.7 km along the satellite track.

The algorithm applied to the ocean backscatter coefficient to infer wind speed is described by Brown et al. (1981). In a 7-month comparison study with the NDBC data set, Dobson et al. (1987) found the Geosat altimeter wind speeds to have a 0.50 m/s low bias with a standard deviation of 1.6 m/s compared to the buoys.

3. STATISTICAL COMPARISON

To compare SSM/I and Geosat wind speed estimates, a data set of collocated measurements has been extracted. This data set is composed of satellite passes that occurred over the world oceans during the first week of August 1987 and have a time difference less than 2 hours. From the 1394-km wide swath, only the SSM/I measurements collocated along the 10-km wide Geosat tracks have been selected. In order to compare the two wind speed estimates over similar size footprint, the altimeter data have been averaged over 4 s which approximately corresponds to a footprint of 10x30 km. Using trial and error, a region around the center of the altimeter footprint of 0.2° x 0.2° in latitude and longitude has been selected as the optimum area over which to average the SSM/I data for comparison with the altimeter wind speed. A total of 25 Geosat and SSM/I passes have thus been selected and a scatter diagram of the wind speed estimates by the two instruments is presented in Figure 1 where 1616 measurements are compared. There is essentially no bias between the two data sets, on the average the altimeter measures winds that are 0.13 m/s higher than the SSM/I, and the standard deviation of the wind speed difference is 1.72 m/s which is of the same order of magnitude as the comparison of each sensor with the NDBC buoy network (Dobson et al., 1987; Goodberlet et al., 1989).

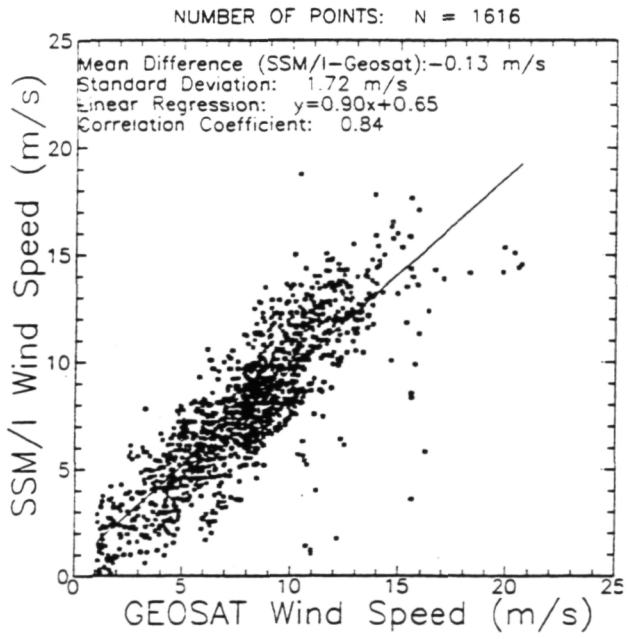

Figure 1: Scatter diagram of SSM/I versus Geosat altimeter wind speed estimates for the global colocated data set with a maximum time interval of 2 hours.

The SSM/I data set consists of wind speed as well as atmospheric parameters estimate (see section 2.1): integrated water vapor (IWV), integrated cloud liquid water (ICLW), index of precipitation (P37), and the ice scattering index (P85). The SSM/I wind speed estimation is only valid in regions with no rain (Goodberlet et al., 1989). According to the values of the precipitation index (P37 < 0.8) , there are only 7 data points in the original data set that are contaminated by rain and should have been eliminated (Table 1). Statistical comparisons as a function of the different atmospheric parameters value derived with SSM/I, show a significant increase in the degree of confidence for data points associated with small amount of integrated cloud liquid water, less than 0.1 kg/m² (Table 1). In cases when ICLW < 0.1 kg/m², the standard deviation of the mean wind speed difference decreases to 1.47 m/s. In intermediate cases of ICLW > 0.1 kg/m² but no precipitation the standard deviation is 1.62 m/s (Table 1).

TABLE 1: Wind speed statistical comparison for collocated Geosat and SSM/I passes with time differences less than 2 hours. N is the number of data points. SSM/I minus Geosat wind speed and the corresponding standard deviation, in parenthesis, are listed in the column labelled SSM/I - Geosat with the correlation coefficient in column CC.

	N	SSM/I-Geosat	CC	
Global data set	1616	-0.13 (1.72)	0.84	(1)
No Rain	1609	-0.15 (1.62)	0.86	(2)
ICLW < 0.1kg/m²	1130	-0.04 (1.47)	0.88	(3)

To check the influence of the time difference between the two satellite passes on the statistical parameters, a new data set with time differences less than one hour has been extracted. The statistics obtained with this new data set are presented Table 2 and Figures 2 and 3. Eighteen passes are now considered with 1056 comparison points where the precipitation index P37 is higher than 0.8 (no rain contamination) (Table 2, line (a)). For data points with less than one hour difference, the standard deviation of the differences decreases from 1.62 m/s (data set with a maximum of 2 hours difference, (Table 1, line (2)) to 1.42 m/s (Table2, line(a), and Figure 2), and from 1.47 m/s (Table 1, line (3)) to 1.18 m/s for pixels with small amount of cloud liquid water (ICLW<0.1 kg/m²), (Table2, line (b), and Figure 3). The decrease in standard deviation shows that part of the discrepancies is due to time differences larger than one hour.

Possible effect of wave height on wind speed differences between the two instruments can be studied using the significant wave height (SWH) measurement by the altimeter. Statistics obtained for three subsets of wave heights are also presented Table 2, lines (a.1) to (a.3). The discrepancy in the statistics between the data sets with waves less than 4 m (Table 2, lines (a.1), (a.2)) and waves higher than 4 m (Table 2, line (a.3)) disappears in the data sets with ICLW<0.1 kg/m² (Table 2, lines (b.1), (b.2), and (b.3)). When there is only small amounts of cloud liquid water in the atmosphere (ICLW < 0.1 kg/m², Table 2, lines(b)), there are no significant differences in the statistical parameters as a function of SWH. A significant difference in the statistical parameters arises when SWH>4 m are associated with amounts of cloud liquid water larger than 0.1 kg/m² which correspond to the crossing of atmospheric fronts, and stormy regions.

TABLE 2: Wind speed statistical comparison for collocated Geosat and SSM/I passes with time differences less than 1 hour. The columns are the same as in Table 1. The statistical comparison is obtained as a function of SWH measured by the altimeter.

	N	SSM/I-Geosat	CC	
No Rain	1056	-0.46 (1.42)	0.88	(a)
0<SWH<2m	463	-0.38 (1.19)	0.84	(a.1)
2<SWH<4m	430	-0.56 (1.26)	0.87	(a.2)
4<SWH<6m	163	-0.41 (2.18)	0.67	(a.3)
ICLW<0.1kg/m²	639	-0.44 (1.18)	0.91	(b)
0<SWH<2m	281	-0.35 (1.09)	0.88	(b.1)
2<SWH<4m	266	-0.58 (1.22)	0.88	(b.2)
4<SWH<6m	92	-0.29 (1.26)	0.84	(b.3)

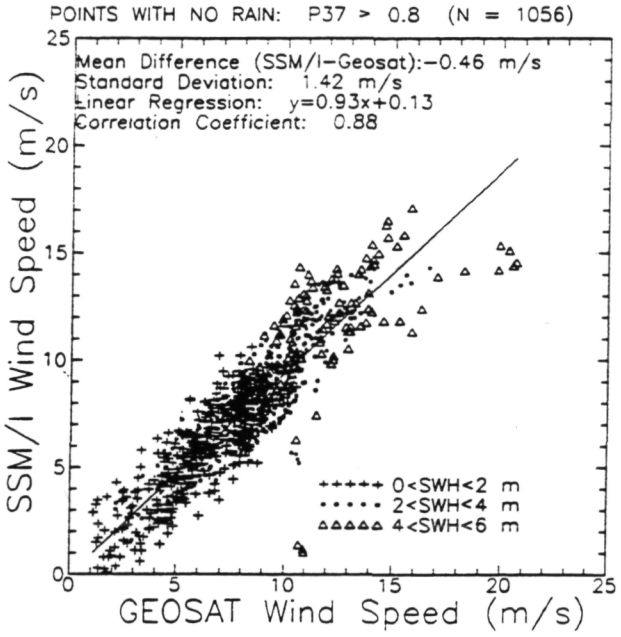

Figure 2: Scatter diagram of SSM/I versus Geosat altimeter wind speed estimates for a maximum time interval of 1 hour. Different symbols display different SWH values derived from the altimeter measurement.

4. EXAMPLE OF QUASI-SIMULTANEOUS MEASUREMENTS BY GEOSAT AND SSM/I

A pass in the North-East Pacific on August 5, 1987, has been chosen to illustrate the quasi-simultaneous measurement by Geosat and SSM/I along the altimeter track. There is only 12 minutes difference between the two satellite passes (Geosat at 0412 UTC and SSM/I at 0424 UTC) and less than 2 hours time difference from the corresponding weather map for 0600 UTC where the Geosat ascending track has been superimposed (Figure 4). The altimeter track starts in a region of relatively moderate winds (ship located at approximately 150°W and 41°N reports 20 kn) then crosses a col with low winds (ship reports 10 kn at 152°W and 45°N) before crossing a cold front at 156°W and 49°N and reaching a region of strong atmospheric pressure gradient behind the front where ships report wind speed between 20 and 35 kn.

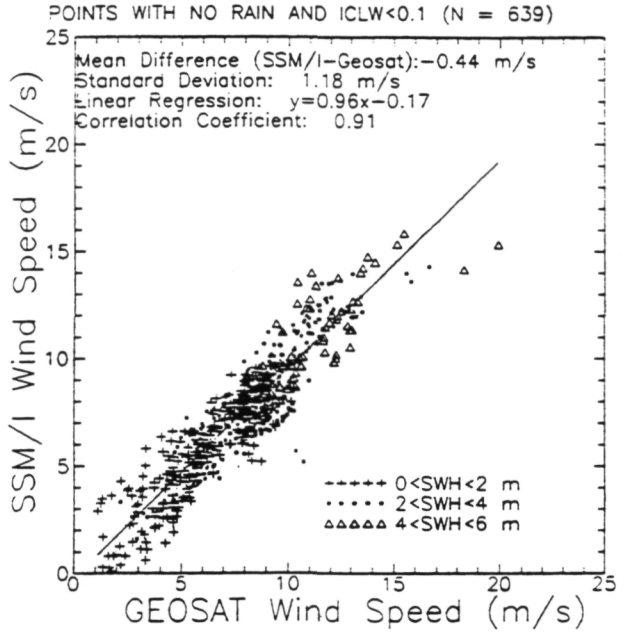

Figure 3: Scatter diagram of SSM/I versus Geosat altimeter wind speed estimates for pixels with small amount of cloud liquid water.

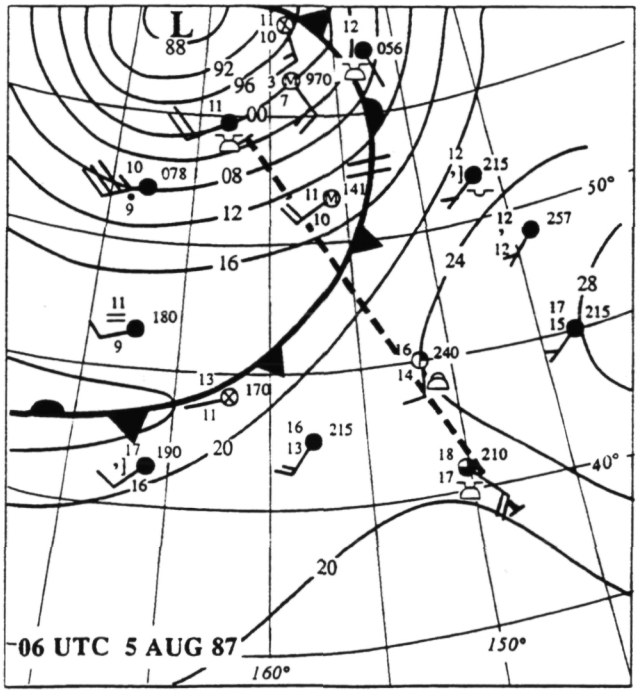

Figure 4: Synoptic weather map with ship reports and Geosat track superimposed (dashed line).

4.1 The SSM/I atmospheric parameters

Figure 5 presents the atmospheric parameter variations derived from SSM/I along the Geosat track. The integrated water vapor variations show the characteristic water vapor maximum in the warm air sector ahead of the cold front, accompanied by a sharp decrease in the cold air mass beyond the front (Figure 5a). The strong water vapor gradient (Figure 5a) located at approximately 48°N is a characteristic feature of the cold front crossing shown on the weather map (Figure 4). The location of SSM/I water vapor gradients

exceeding 0.1 (kg/m²)/km provides an excellent objective indication of the location of many surface cold fronts (Katsaros et al., 1989) as is the case here. The precipitation index (P37), which may be interpreted as a measure of the visibility of the polarized sea surface through cloud and precipitation (Petty, 1990) exhibits a similar feature as the IWV with a strong gradient located at about 49°N (Figure 5b). This gradient corresponds to a region with P37 < 0.8 indicating heavy precipitations during the crossing of the frontal zone. Another region of heavy rain is behind the front between 52 and 54°N. The calm region of the col south of the front (Figure 4) from about 44 to 47°N corresponds to precipitation-free pixels with P37 of the order of 0.95. P37 values between 0.8 and 0.9, imply at most light precipitation. The vertically integrated cloud liquid water variations along the Geosat track are presented in Figure 5c. In the region of the front crossing, the ICLW have been flagged because of heavy precipitation. South of the front, the col is the region with no precipitation (P37 < 0.9) and little cloud liquid water (ICLW < 0.1 kg/m²). The region of precipitation (P37 < 0.8) north of the front corresponds to ICLW between 0.28 and 0.34 kg/m². Everywhere else, the values of ICLW vary between 0.1 and 0.3 kg/m², an indication of diverse cloud structures

4.2 SSM/I and altimeter wind speed comparison

SSM/I and Geosat both measure sea surface wind speed. The wind speed and significant wave height variations measured by the altimeter are presented in Figure 6. At the start of the pass (southward), the altimeter measures 2 m waves and 9 m/s wind speed in agreement with the 20 kn ship report in the vicinity. The crossing of the col is signaled by very low wave (about 1 m) and by low winds varying between 1 and 5 m/s. In the North, the crossing of the cold front is marked by a wind speed increase from 5 to 10 m/s and a region where waves increase to 2 m. Gradients of wind speed and wave height are measured to the north, beyond the cold front, across the atmospheric pressure gradient zone. In section 4.1, the portions of the pass affected by heavy rains (across the front and in part of the region of strong atmospheric pressure gradient) where the SSM/I wind speed cannot be derived are discussed. In the portions with no heavy precipitation, an estimate of the SSM/I wind speed is obtained and plotted in Figure 7 along with the Geosat estimates. A very good global agreement is obtained especially in regions of wind gradients. Only in the southern portion of the pass does SSM/I measure slightly higher winds than Geosat. Part of these discrepancies can be accounted for by the differences in footprint size between the two sensors.

5. CONCLUSION

A comparison of colocated wind speed measurements by the Geosat altimeter and the SSM/I within a 2-hour time frame yields a statistical agreement of the same order of magnitude as was obtained for the comparison of the individual satellite sensors with the NDBC buoy network (Dobson et al., 1987; Goodberlet et al., 1989; Figure1; Table 1). There is no significant bias between altimeter and SSM/I wind speed and a standard deviation of 1.62 m/s after complete elimination of rain pixels (Table 1, line(2)). When the time frame for the comparison is reduced to 1 hour, the number of data points decreases by about one-third, the altimeter has a 0.5 m/s high bias compared to the SSM/I and the standard deviation decreases to 1.42 m/s for the global data set and to 1.18 m/s for conditions when there is little cloud liquid water (ICLW < 0.1 kg/m²). The agreement between the two satellite sensors under favorable atmospheric conditions is much better than the

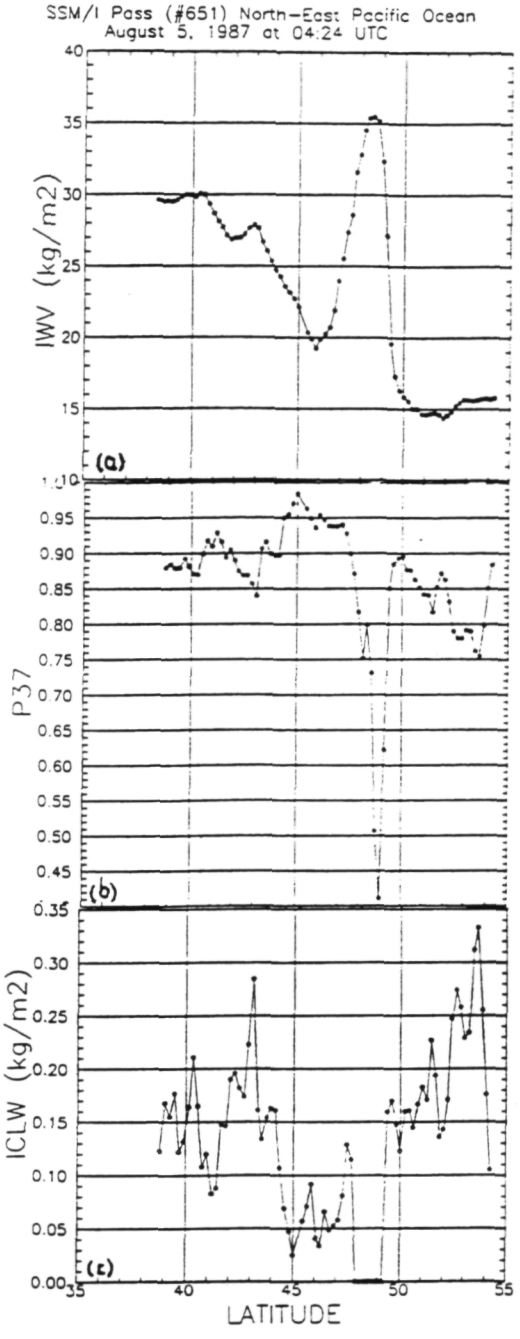

Figure 5: Variations of atmospheric parameter estimates from SSM/I along the Geosat track; (a) integrated water vapor variations; (b) precipitation index; (c) integrated cloud liquid water (pixels where ICLW could not be estimated are arbitrarily set to zero).

agreement of the individual instruments with the buoy network. This should not be too surprizing since both Geosat and SSM/I measure spatially averaged wind speeds over regions of 30-50 km size over a time interval of a few seconds while buoys measure time averaged winds (over several minutes) in one point location. The effect of wave height on the statistics is negligible away from storms (ICLW < 0.1 kg/m²) in regions where sea state is swell dominated (Table 2). In the vicinity of storms atmospheric and maybe sea state effects are responsible for the poor correlation between the two wind speed measurements and for the standard deviation increase (Table 2, line (a.3)).

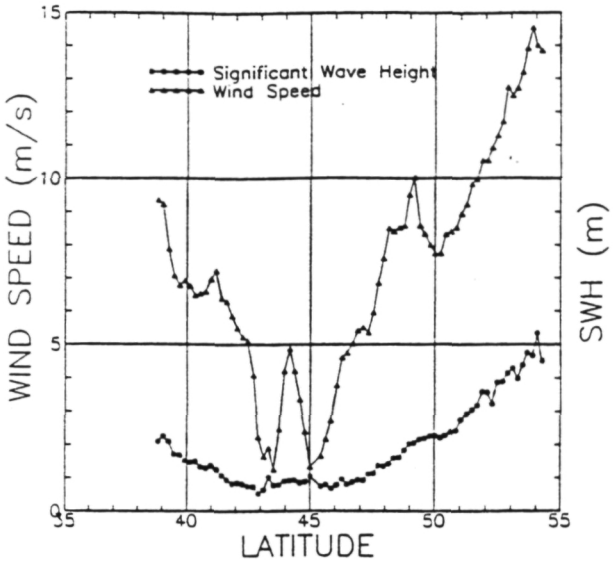

Figure 6: Geosat radar altimeter wind speed and significant wave height (SWH) estimates.

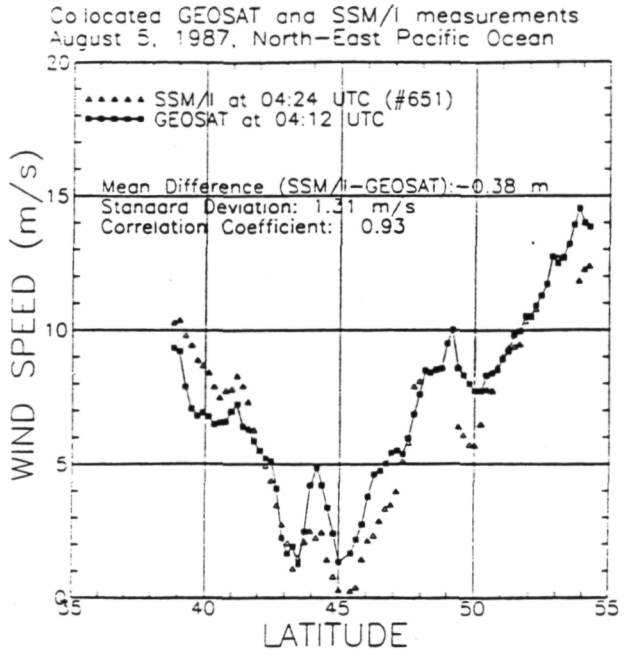

Figure 7: Geosat and SSM/I wind speed variations at 19.5 m above sea level.

The quasi-simultaneous Geosat and SSM/I measurements across a region of low winds, then across a cold front and in the region of strong atmospheric pressure gradient behind the front demonstrate the ability of both instruments to accurately locate and measure atmospheric and sea state gradients. In regions with little or no precipitation, the two wind speed estimates have a correlation coefficient of 93%. Compared to buoys or ship reports of wind, the satellite winds have better or comparable accuracy and are the only instruments able to provide ocean wide gradients (Geosat and SSM/I) and fields (SSM/I) of atmospheric or sea state parameters. These satellite measurements should be used in combination with in situ measurements and models to improve our understanding of the interactions between the atmosphere and the ocean.

Acknowledgments: This work was performed under NASA Grant NAGW 1688 to the University of Washington. We thank Jennifer Miletta and Hongwei Zhao for assistance with data retrieval and Ms. Kay Dewar for drafting of the weather map.

REFERENCES

Brown, G.S., H.R. Stanley, and N.A. Roy, 1981, The wind speed measurements capability of spaceborne radar altimeters, IEEE J. Oceanic Eng., 6 (2), p. 59-63.

Claud, C., N.M. Mognard, K.B. Katsaros, A. Chedin, N.A. Scott, 1991, Satellite observations of polar lows by SSM/I, Geosat and TOVS, Proceedings of the IGARSS'91 Symposium held in Hesinski, Finland, June.

Dobson, E., F. Monaldo, J. Goldhirsh, and J. Wilkerson, 1987, Validation of Geosat altimeter-derived wind speeds and significant wave heights using buoy data, Johns Hopkins APL Tech. Rep., 8, 2, p. 222-233.

Goodberlet, M.A., C.T. Swift, and J.C. Wilkerson, 1989, Remote sensing of ocean surface winds with the Special Sensor Microwave/Imager, J. Geophys. Res., 94, p. 14,547-14,555.

Hollinger, J., R. Lo, G. Poe, R. Savage, and J.Pierce, 1987, Special Sensor Microwave/Imager User's Guide, Naval Res. Lab., Wash. D.C., 177 pp.

Katsaros, K.B., I.A. Bhatti, L.A. McMurdie, and G. Petty, 1988, Identification of atmospheric fronts over the ocean with microwave measurements of water vapor fields and rain, Weather and Forec., 4, 4, p. 449-460.

Mc Arthur, J.L., P.C. Marth Jr., J.G. Wall, R.V. Sailor, and A.R. LeSack, 1987, The Geosat radar altimeter, Johns Hopkins APL Tech Dig. 8,2, p. 176-181.

Mognard, N.M. and W.J. Campbell, 1984, Comparison of Sea Surface Wind Speed Fields by SEASAT Radar Altimeter, Scatterometer, and Scanning Multichannel Microwave Radiometer, with an Emphasis on the Southern Ocean, Proceedings of IGARSS'84 Symposium, ESA SP-215, Strasbourg, France, 27-30 August, p. 403-409.

Mognard, N.M., and K.B. Katsaros, 1990, Evolution of atmospheric fronts over the ocean as observed with the Special Sensor Microwave/Imager and the Geosat altimeter, Proceedings of the 5th Conference on Satellite Meteorology and Oceanography, Sep. 3-7, p. 118-122

Petty, G.W., 1990, On the response of the Special Sensor Microwave/Imager to the marine environment. Implications for atmospheric parameters retrievals, Ph.D. dissertation, U. of Washington, 291 pp.

Petty, G.W., and K.B. Kataros, 1990a, New geophysical algorithms for the Special Sensor Microwave Imager, Proceedings of the 5th International Conference on Satellite Meteorology and Oceanography, Sept. 3-7, London, p. 247-251.

Petty, G.W., and K.B. Kataros, 1990b, Precipitation observed over the South China Sea by the Nimbus-7 Scanning Multichannel Microwave Radiometer during winter MONEX, J. Appl. Meteor., 29, p. 273-287.